




Synthesis and optoelectronic characterization of coronene/CdO self-powered photodiode

Fatih Unal^{1,*} , Mustafa Sukru Kurt², Sitki Aktas³, and Mehmet Kabaer⁴

¹Central Research Laboratory, Application and Research Center, Giresun University, Giresun, Turkey

²Department of Fundamental Science, Science Faculty, Erzurum Technical University, Erzurum, Turkey

³Department of Mechanical Engineering, Faculty of Engineering, Giresun University, Giresun, Turkey

⁴Department of Physics, Faculty of Science and Art, Giresun University, Giresun, Turkey

Received: 19 July 2022

Accepted: 28 September 2022

Published online:

9 October 2022

© The Author(s), under exclusive licence to Springer Science+Business Media, LLC, part of Springer Nature 2022

ABSTRACT

In this study, it is aimed to present the coronene/CdO hybrid heterojunction, which has not been grown epitaxially on each other before, as an alternative to optoelectronic application areas. Firstly, CdO thin film was grown on a conductive layer (ITO) using the electrochemical deposition method. Then, coronene organic semiconductor was grown on CdO thin film using thermal evaporation method and coronene/CdO hybrid heterojunction was produced. The optical analysis of the fabricated heterojunction was examined in the wavelength range of 300–850 nm, and optical parameters were determined. It was observed that the the absorption coefficient (α) value of the heterojunction was in the order of $\approx 10^6 \text{ m}^{-1}$ and the E_g value (2.01 eV) was in the visible region. The diode parameters of the coronene/CdO hybrid heterojunction which showed negative differential resistance (NDR) effect behavior were determined, and it was observed that the ideality factor value was 7.58, the series resistance value was $\approx 10^3 \Omega$, the shunt resistance value was $\approx 10^5 \Omega$, the barrier height value was $\approx 0.3 \text{ eV}$, and the reverse saturation current value was $\approx 10^{-8} \text{ A}$. The photodetector and photovoltaic characterization of the coronene/CdO hybrid heterojunction at different light intensity values was investigated under $\pm 0.1 \text{ V}$ and with zero bias. It is observed that it exhibited self-powered diode behavior under zero bias and the heterojunction was light-sensitive. The determined maximum photocurrent (I_{ph}), responsivity (R), sensitivity and specific detectivity (D^*) values were found to be $2.03 \times 10^{-7} \text{ A}$, $1.53 \times 10^{-2} \text{ A.W}^{-1}$, $7.44 \times 10^{-8} \text{ S.m.W}^{-1}$ and $9.94 \times 10^9 \text{ Jones}$, respectively. In addition, the I_{sc} and V_{oc} values increased with the increase in the light intensity and the maximum FF% value was 31.14%.

Address correspondence to E-mail: fatih.unal@giresun.edu.tr

1 Introduction

The needs of continuously developing optoelectronic technology have attracted considerable interest from the academy and industry to develop more efficient and alternative transparent metal oxide semiconductor materials. For this purpose, researchers have been engineering various materials and designs in order to exceed the limits of metal–semiconductor contacts that are used in many applications in the electronics industry such as solar cells, light-emitting diodes, photodetectors, phototransistors, liquid crystal display, gas sensors and photocatalytic. [1–8]

Among these metal oxide semiconductors, cadmium oxide (CdO) is an II–VI group n-type semiconductor with direct band gap ranges from 2.2 to 2.6 eV [9]. CdO is promising thanks to its electrical, optical and magnetic properties as well as good chemical stability. Also features such as low cost and ease of fabrication, large carrier concentration, high mobility and potentially large optical response range make the potential for extensive usage and investigation. As is known, CdO thin films are produced with different techniques such as sol–gel spin coating [10], magnetron sputtering [11], thermal evaporation [12], hydrothermal [13, 14] and electrodeposition [15] techniques. The electrochemical deposition technique came up with appealing features such as being capable of growing high-purity and homogenous films on desired surfaces with ease, simple and very cheap way that makes it an important method compared with others.

The interface of two different materials known as heterojunction always plays an important role in optoelectronic applications. Therefore, a coronene layer was coated on the CdO thin film. Coronene is a molecule formed by the combination of six benzene rings arranged in a loop. It shows two different crystal structures depending on the temperature and pressure [16]. Coronene is a yellow-colored molecule with the formula $C_{24}H_{12}$. The molar mass of coronene is 300.36 gr/mol, its density is 1371 gr/cm³, melting point is 437.3 °C, the boiling point is 525 °C, vapor pressure is 2.17×10^{-12} mmHg, and decomposition temperature is 500 °C 3Gpa [17, 18].

Coronene is a π -linked semi-condensed PAH with a high degree of D_{6h} symmetry [16, 19]. Only a few articles reported heterojunction structures with coronene. El-Nahass et al. [19] investigated photovoltaic behavior and electrical characterization of coronene/

p-Si heterojunction fabricated under temperatures varied from 292 to 373 K. Erdal [20] studied the characterization of Al/CRNNW/n-Si device with a coronene nanowire (CRNNW) interlayer by I–V measurements for photodiode applications under dark and various illumination intensities. Xiao et al. [21] obtained a strong photocurrent response produced by the thin film of coronene nanowires on the rGO/SiO₂/Si electrode. Additionally, they fabricated a heterojunction LED device with the structure of quartz/ITO/p-coronene nanowires/n-SiC/ Ti (10 nm)/Au (120 nm) and found that diodes using organic nanowires as the *p*-type hole injection layer show better electroluminescence emission performance than those with only inorganic thin-film structures. Additionally, F. Unal [22] investigated optoelectronic properties of coronene deposited on electrochemically grown InSe, CuInSe (CIS) and CuInGaSe (CIGS) inorganic semiconductor thin films and received promising results at optoelectronic application area. However, the effects of coronene organic layer deposited on transparent metal oxide on optoelectronic devices are limited in the literature. Hence, It was aimed to investigate several optical and electrical parameters of coronene/CdO heterojunction as an alternative to optoelectronic circuit elements.

2 Materials and methods

Inorganic and organic layers of heterojunction were grown on indium tin oxide (ITO) surface by electrochemical deposition and thermal evaporation techniques as schematically illustrated in Fig. 1. Firstly, the ITO/glass substrate with dimensions of 2 to 1 cm was cleaned using acetone, methanol and propanol in an ultrasonic bath for 10 min, respectively. Substrates were finally dried by blow-drying with nitrogen gas.

Inorganic CdO thin-film structure was electrochemically deposited on the ITO/glass substrate by applying -0.7 V during 3600 s at 70 °C (based on our internal study) using the Metrohm Autolab PGSTAT128N system. Deposition parameters were determined based on our internal studies. The electrolyte solution contains 5 mM Cd(NO₂)₃·4H₂O (30 ml) and 250 mM LiCl (10 ml). Three-electrode configuration was designed using the ITO as the working electrode, the Pt plate as the counter electrode and the Ag/AgCl reference electrode.

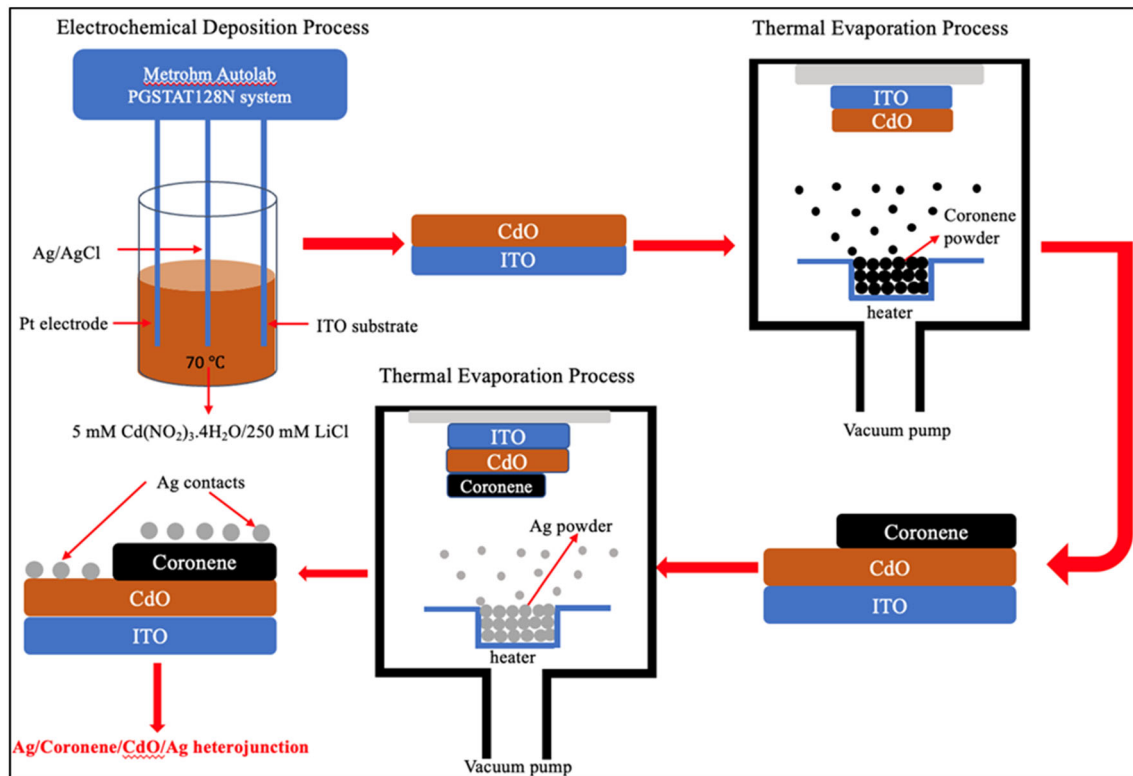


Fig. 1 Schematic representation of a growing process of Ag/coronene/CdO/Ag heterojunction

Coronene organic molecule was grown on an electrochemically deposited CdO surface by a thermal evaporation method using the Vaksis (PVD-MT/2M2T) system. The process was carried out at room temperature under high-vacuum conditions ($\sim 10^{-6}$ Torr). Additionally, Ag contacts were deposited on CdO and coronene surfaces by the thermal evaporation method and are illustrated in Fig. 1 Ag/coronene/CdO/Ag hybrid heterojunction was fabricated.

The structural pattern of the CdO structure was determined using an X-ray diffractometer (XRD) (GNR Europe 600 XRD) using Cu-K α (1.5418740 Å) radiation from 20° to 70°. Surface morphology and film thicknesses of CdO and coronene thin films were investigated by Scanning electron microscopy (SEM). The elemental composition of the electrochemically deposited film was examined by energy-dispersive X-ray spectrometry (EDX). Also, optical and electrical characterization of the hybrid heterojunction was performed using the Hach DR600 model UV–Vis spectrometry and I–V characterization system (FYTRONIX Solar Simulator LSS 900 Characterisation System), respectively.

3 Results and discussion

3.1 Structural analysis

XRD pattern of the electrochemically deposited CdO thin film is shown in Fig. 2. CdO adapted to the cubic phase in the CdO/ITO/glass thin film with the parameters (entry # 96-900-6684) Fm-3 m (225) and

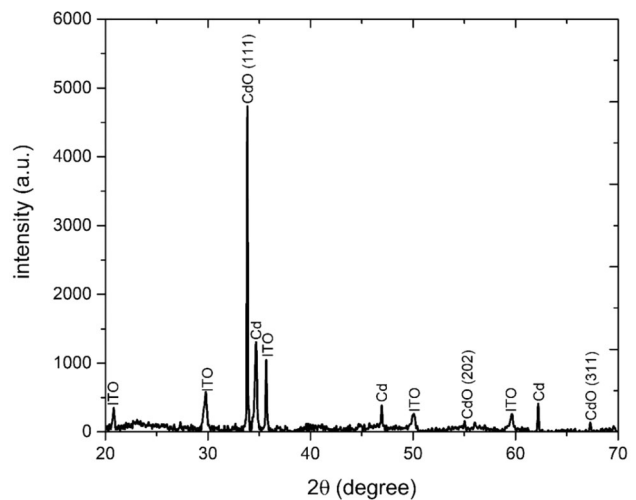


Fig. 2 XRD pattern of CdO thin film grown on ITO/glass

$a = 4.61900 \text{ \AA}$. It was observed that the CdO phase has grown on (111), (202) and (311) planes with 2θ values of 33.58, 56.29 and 67.16, respectively. Additionally, metallic Cd peaks were obtained from XRD peaks at 2θ values of 34.66, 46.92 and 62.24 degrees. The reason for the metallic Cd peaks observed in the XRD spectrum can be explained is due to the non-annealing of the thin film [23].

SEM images of electrochemically deposited CdO surface at 2000 and 10,000 magnifications are illustrated in Fig. 3a and b, respectively. It is obvious that CdO particles with various dimensions from 500 nm to 2.0 μm were formed at irregular-shaped morphology essentially with a small amount of agglomeration. Besides, almost all of the ITO surface was homogeneously covered by CdO particles and a generally rough surface was formed. Figure 3c and d shows the top view of the coronene which was deposited on the CdO surface at 2 and 10 K magnifications, respectively. It can be said that the thickness and the length of coronene wire varied from 150 to

300 nm and 2.0 to 5.0 μm , respectively. Also, the density of coronene wires deposited on the CdO surface was homogeneously distributed. Additionally, cross-sectional SEM images of CdO and coronene thin-film layer are demonstrated in Fig. 4. The average thicknesses of CdO and coronene films (measured at five random regions) were determined as 1.32 and 1.41 μm , respectively. A high-magnification image of coronene wires at various dimensions (see Fig. 3d) revealed that the coronene wires heavily horizontally grew on the CdO surface. Although the lengths of the coronene wires vary between 2.0 and 5.0 μm , the reason for the cross-sectional thickness of 1.47 μm can be shown as the intense horizontal growth of the wires.

The purity and the presence of elements of electrochemically grown CdO film were examined with the EDX spectrum demonstrated in Fig. 5. Figure 5 reveals that CdO film has a Cd/O weight ratio of 60.3/39.7. Additionally, no other elements were observed from the EDX spectrum and the results

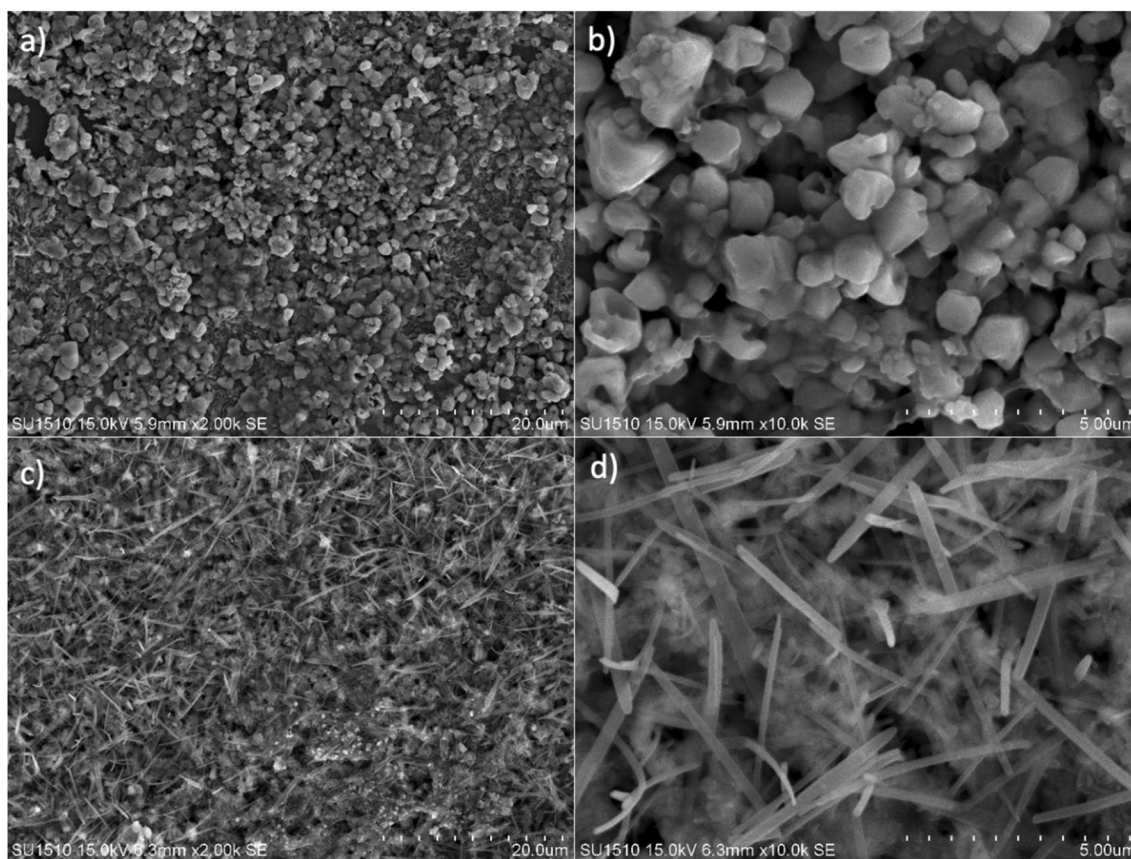


Fig. 3 a and b SEM images of CdO thin-film structure at 2000 and 5000 magnifications. c and d SEM image of coronene organic structure at 2000 and 5000 magnifications

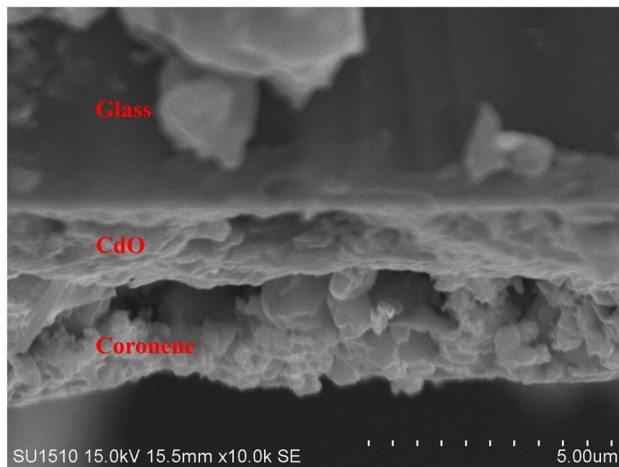


Fig. 4 Cross-sectional SEM image of CdO and coronene thin films deposited by electrochemical and thermal evaporation methods

confirm that electrochemically deposited CdO film had high purity.

3.2 Optical analysis

In optoelectronic applications, the optical characteristics of thin films formed as heterojunctions on one another are critical [24–26]. To establish their appropriateness for optoelectronic applications, the optical characteristics of the fabricated coronene/CdO/

ITO/glass heterojunction worth to be investigating. Optical parameters such as the absorption coefficient (α), optical transmittance (%T), reflectance (%R), forbidden energy bandgap (E_g), optical conductivity (σ), refractive index (n), extinction coefficient (k), real (ϵ_r) and imaginary dielectric constants (ϵ_i), and dielectric loss (ϵ_i/ϵ_r) of first-time fabricated glass/ITO/coronene/CdO hybrid heterojunctions were investigated in detail between the 300 and 850 nm wavelength range.

α is calculated using the following formula,

$$\alpha = \frac{2.303 \cdot A}{t} \quad (1)$$

where A and t represent to absorbance and thickness of the film, respectively. The bandgap of the forbidden energy is calculated using optical absorption spectrometry. The relationship between the absorption coefficient and the energy bandgap (E_g) is given as follows [27].

$$\alpha(h\nu) \approx (h\nu - E_g)^n \quad (2)$$

where $h\nu$ is photon energy and n is $\frac{1}{2}$ for direct allowed transitions. E_g is calculated by extrapolating the straight-line section of the plot to the energy axis using plots of $((\alpha h\nu)^{\frac{1}{n}})$ versus $h\nu$. The value of E_g is then determined by the intercept.

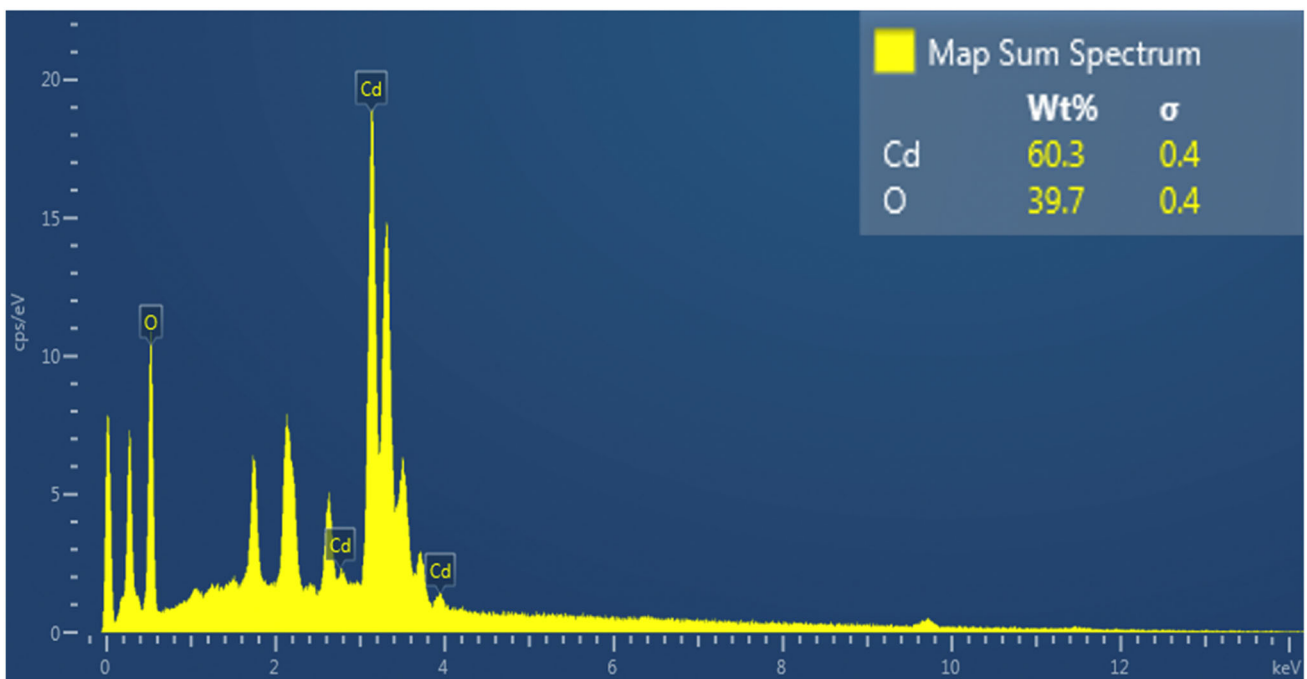


Fig. 5 EDX spectrum of electrochemically grown CdO film

Figure 6a shows the graph of absorbance coefficients as a function of wavelength for heterojunction. The coronene/CdO/ITO/glass heterojunction exhibits strong absorption across the spectrum, as shown in Fig. 6a, with the highest peak at 305 nm having a value of $1.15 \times 10^6 \text{ m}^{-1}$. The graph of $h\nu$ versus $(\alpha h\nu)^2$ is shown in Fig. 6b. A band gap of $2.33 \pm 0.15 \text{ eV}$ was observed for the heterojunction, which is lower than the band gap values of the coronene thin film grown on InSe CIS (2.69 eV), CIGS (2.87 eV) and InSe (3.09 eV)[22]. The fact that the calculated E_g value is lower than the values in the literature is related to the crystallization of the coronene grown on different substrates.

The equation for the relationship between absorbance (A) and transmittance (T) is:

$$A = -\log T \tag{3}$$

The transmittance T of the film is expressed as below formula when the multiple reflections are neglected [28]:

$$T = (1 - R)^2 \exp(-A) \tag{4}$$

where R is the reflectance and could be calculated from T and A parameters using Eq. 4 and can be rearranged as follow:

$$R = 1 - \left(\frac{T}{\exp(-A)} \right)^{1/2} \tag{5}$$

Figure 7a shows plots of transmittance (T%) (black line) and reflectance (R%) (blue line) as a function of

wavelength (λ) for the coronene/CdO/ITO/glass heterojunction. The coronene/CdO/ITO/glass heterojunction has a transmittance of 9.98% at maximum wavelength and drops to almost half of its value in the absorption region with a value of 5.11%. The decrease of T% values toward the absorption region indicates that the heterojunction has an absorbent nature. Additionally, the heterojunction exhibits the highest reflectance with a value of 9.02% about 305 nm wavelength (absorption region), then gradually decreases to 8.54% for the highest wavelength (see Fig. 7a).

The following formula is used to calculate the relationship between the absorption coefficient (α) and the extinction coefficient (k):

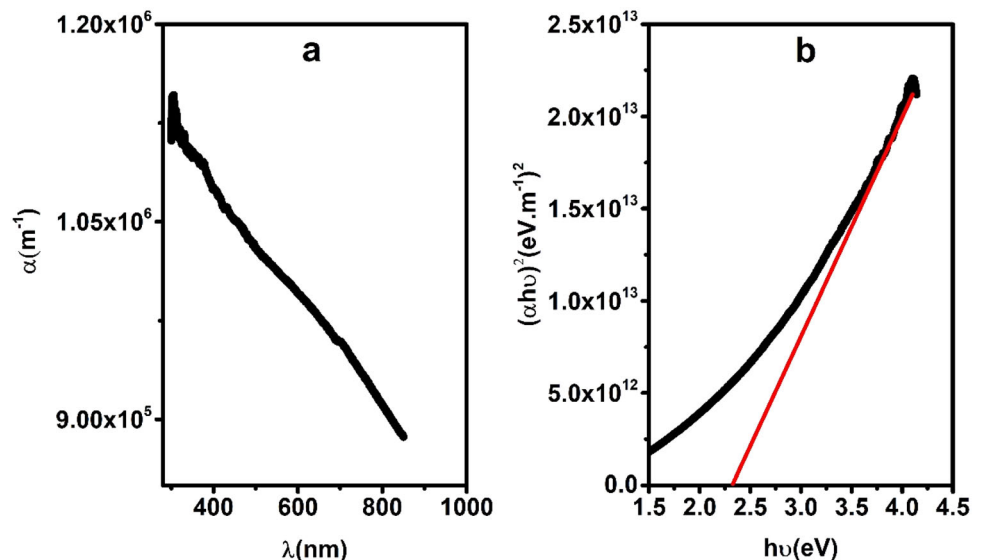
$$k = \frac{\lambda \cdot \alpha}{4\pi} \tag{6}$$

The refractive index (n) is then calculated as follows [28]:

$$n = \frac{1 + R}{1 - R} + \sqrt{\frac{4R}{1 - R^2} - k^2} \tag{7}$$

Figure 7b shows the plots of extinction coefficient (k) (black line) and refractive index (n) (blue line) values as a function of wavelength (λ) for the coronene/CdO/ITO/glass heterojunction. Figure 7b shows that the maximum k value is observed around 1.46 eV ($\approx 850 \text{ nm}$) photon energy with a value of 0.06, and then rapidly decreases to the lowest value of around ≈ 0.026 for 4.15 eV ($\approx 300 \text{ nm}$) photon energy. The n values of heterojunction are highest

Fig. 6 a Absorption coefficients (α) of coronene/CdO/ITO/glass as a function of wavelength and b plot of $(\alpha h\nu)^2$ versus photon energy



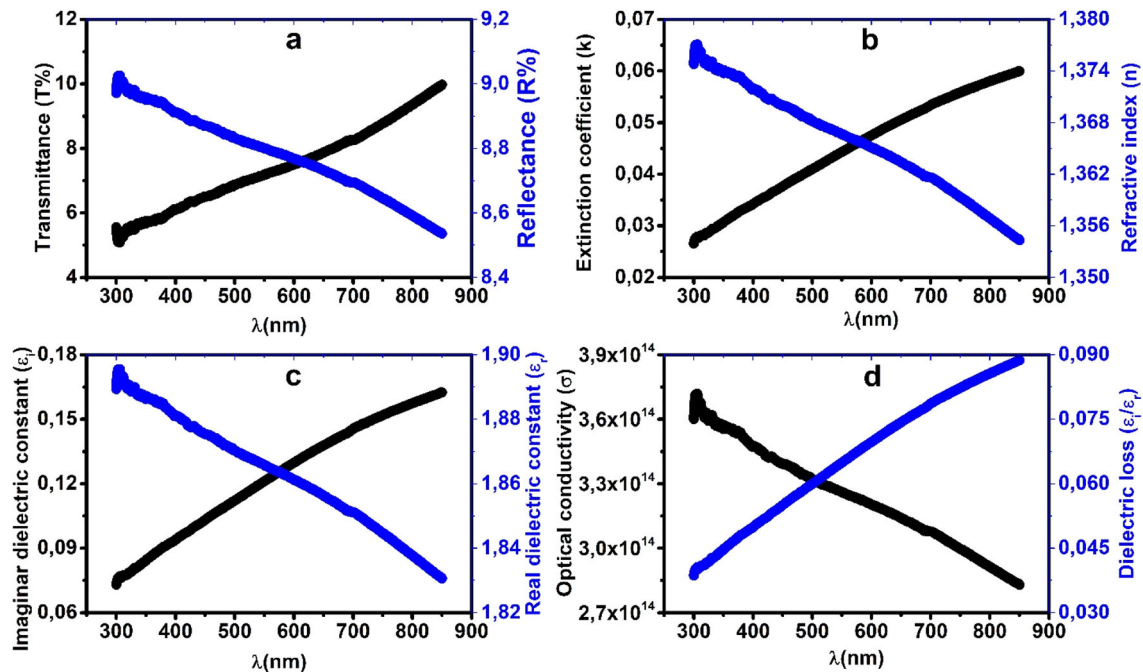


Fig. 7 **a** Transmittance (T%) and reflectance (R%), **b** extinction coefficient (k) and refractive index (n), **c** imaginary (ϵ_i) and real dielectric (ϵ_r) constants and **d** optical conductivity (σ) and

dielectric loss (ϵ_i/ϵ_r) of the coronene/CdO/ITO/glass heterojunction versus to the wavelength

around 4.1 eV (≈ 303 nm) photon energy with a value of 1.377, then gradually decrease to around the value of 1.354 for the lowest photon energy 1.47 eV (≈ 845 nm). $\epsilon_r = n^2 - k^2$, $\epsilon_i = 2nk$, ϵ_i/ϵ_r and $\sigma = \alpha nc/4\pi$ are the real and imaginary components of the dielectric constant, dielectric loss and optical conductivity, respectively. Figure 7c shows the plots of imaginary (ϵ_i) (black line) and real dielectric (ϵ_r) (blue line) constants as a function of wavelength (λ) for the coronene/CdO/ITO/glass heterojunction. The imaginary dielectric constant reaches its highest value of 0.163 around 305 nm wavelength and then drops to 0.073 almost following the linear trend as wavelength approaches the absorption region. In contrast to the imaginary dielectric constant, the real dielectric constant steadily drops as the wavelength increases, from a maximum of 1.895 at 305 nm wavelength to 1.830 at the highest measured wavelength value again following a linear trend in the opposite direction with the imaginary dielectric constant. Figure 7d shows the relationship between optical conductivity and dielectric loss for the coronene/CdO/ITO/glass heterojunction as a function of wavelength (λ). The optical conductivity of heterojunction decreases steadily from 3.71×10^{14} at the 305 nm wavelength to the value of 2.83×10^{14} for

the highest wavelength. On the other hand, the dielectric loss of heterojunction increases sharply from the absorption region with the value of 0.039 to 0.089 for the highest wavelength.

3.3 Electrical analysis

The I–V characteristics of Ag/coronene/CdO/Ag hybrid heterojunction were investigated within the ± 3 V potential range in the dark environment. The conventional I–V graph of Ag/coronene/CdO/Ag hybrid heterojunction is given in Fig. 8a. As shown in Fig. 8a, the heterojunction showed typical rectifying characteristics and the current increased easily under forward bias, while the current was cut off under reverse bias due to the barrier height and the expansion of the depletion region between the CdO and coronene layers. The rectification ratio RR ($RR = I_{\text{forward}}/I_{\text{reverse}}$)[29] of Ag/CdO/coronene/Ag hybrid heterojunction was found to be $\approx 0.7 \times 10^2$ at 3 V potential. Compared to the literature, this ratio was found to be higher than coronene/p-Si-based heterojunctions, n-VO₂/n-MoSe₂ heterojunction diode and p-Si/Fe(II)-polymeric complex/Au diode in a dark environment [30–32]. In Fig. 8b, a, semilogarithmic I–V graph of Ag/coronene/CdO/

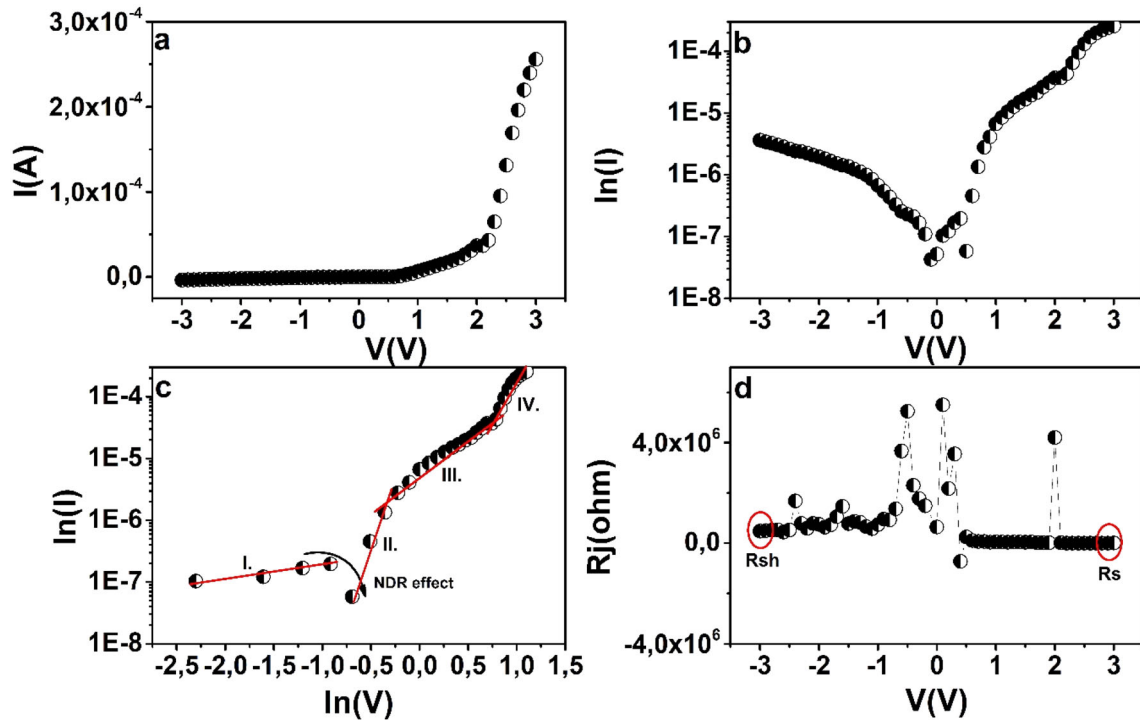


Fig. 8 Graphs of Ag/coronene/CdO/Ag hybrid heterojunction **a** I–V, **b** semilogarithmic I–V, **c** double logarithmic I–V and **d** Rj–V

Ag hybrid heterojunction is given. It is seen that for both reverse and forward bias current values have an asymmetry and under the reverse bias, a non-saturated state exists. On the contrary, the current did not remain constant as expected and raised with the increase in the reverse bias voltage. This can be explained by interface states and barrier height reducing image forces [33–35]. Since, image charges form on the metal electrode of the metal–semiconductor junction as the carriers approach the metal–semiconductor interface. The potential of these charges lowers the effective barrier height. It increases the current while decreasing the barrier height [36]. Under the forward bias, the current increased in the potential range of 0–0.4 V, and the current decreased significantly at 0.5 V while the current decreased against the increasing voltage. This phenomenon is referred to as negative differential resistance (NDR) [37]. As the external electric field strength acting on the structure increases, which depends on the applied potential difference, the band overlaps between CdO and coronene layers are partially disappeared or decreased. In other words, there has been a decrease in the number of electrons contributing to the current quantum mechanically, which has led to a decrease in the current against increasing

voltage [38]. This state is the working principle of tunnel diodes [39] and gun diodes [40]. The NDR effect was reported by Rehman et al. [41] in BaTiO₃/CeO₂ heterostructure also Li et al. [42] observed in dipyrimidinyl–diphenyl molecular junctions, and while it is seen in inorganic/inorganic, organic/organic heterojunctions in the literature, this behavior was seen for the first time in coronene/CdO-based heterojunctions. As the values go higher than 0.5 V, the series resistance starts to show its effect. In order to understand the dominant current transmission mechanism of Ag/coronene/CdO/Ag hybrid heterojunction better, a double logarithmic I–V graph under forward bias is given in Fig. 8c. There are different transmission mechanisms, namely I, NDR, II, III and IV regions, and in these regions with different slopes, ohmic, space-charge-limited current (SCLC), trap filling limit (TFL) and trap-free SCLC transmission mechanisms are available, respectively [43–45]. The current in these regions depends on the potential with the relation $I \approx V^m$ [34] and m denotes the slope. The m values of Ag/coronene/CdO/Ag hybrid heterojunction in regions I, II, III and IV are 0.20, 4.09, 1.12 and 3.28, respectively. The low-voltage region, namely region I ($-2.30 < \ln V < -0.91$), has ohmic behavior, and since the injected effective

carrier density is lower than the background thermal carrier density, an ohmic mechanism is controlled where current increases smoothly with voltage [46] and this state is related to the distribution of traps. The dominant mechanism in region II ($-0.69 < \ln V < -0.35$) is SCLC. The voltage becomes more significant than in the previous region, and the density of injected free carriers is considerably higher than that of thermally generated carriers [47], which leads to a sharp increase in current. The dominant mechanism in region III ($-0.22 < \ln V < 0.74$) is TFL. Here, deep trap levels are filled with injected electrons [48]. The region IV ($0.78 < \ln V < 1.09$) is the high-voltage region and although voltage values are higher in these region, the slope is lower than the slope of the region II. The dominant transmission mechanism in the high-voltage region is trap-free SCLC. Here the traps are filled with injected electrons and current transmission is described by the trap-free Mott–Gurney law [48, 49].

Series resistance (R_s) and shunt resistance (R_{sh}) are very important parameters in heterojunctions that show diode characteristics. In order to determine these parameters, the junction resistance can be determined from the graph of R_j ($R_j = dV/dI$) drawn against the applied potential based on Ohm's law. R_j value that remains almost constant in the high-reverse-bias-voltage region gives us the value of R_{sh} , while the value of R_j that remains almost constant in the high-voltage region of forward bias gives us the value of R_s [50]. In Fig. 8d, the graph of the joint resistance R_j of Ag/coronene/CdO/Ag hybrid heterojunction against potential is given. While the R_{sh} value of Ag/CdO/coronene/Ag hybrid heterojunction was $5.3 \times 10^5 \Omega$, the R_s value was determined as $2.6 \times 10^3 \Omega$. Diode parameters of Ag/coronene/CdO/Ag hybrid heterojunction such as ideality factor (n), barrier height (ϕ_b), series resistance (R_s) and reverse saturation current (I_0) can be determined based on current–voltage characterization by using different methods [29, 33, 51–53]. The diode parameters calculated using the conventional method [54] and the Cheung–Cheung functions [55] are given in Table 1. The calculated n values are far from the ideal diode with a value of 1. The formation of unwanted oxide layers during the experiment, the effect of series resistance, impurities and inhomogeneous distribution of the charges in the layers can cause this state [34, 56]. There are differences in the

values calculated by different methods. The reason for this is that while calculations were made by considering the low-voltage region in the conventional method, calculations were made over the low- and medium-voltage region in the Cheung–Cheung method.

3.3.1 Photodetector and photovoltaic analysis

In Fig. 9, the I–V characteristics of Ag/coronene/CdO/Ag hybrid heterojunction at room temperature under dark and light intensity of 20, 40, 60, 80, 100 $\text{mW}\cdot\text{cm}^{-2}$ are given. Figure 9 shows that the Ag/coronene/CdO/Ag hybrid heterojunction is light-sensitive, and the conductivity increases with the effect of light under reverse and forward bias. Photons with higher energies than the forbidden energy band gap lead to the formation of new electron–hole pairs at the depletion region boundaries between the CdO and coronene layers. Stress formation under light causes an internal electric field at the grain boundaries. This internal electric field forces electrons and holes to separate from each other. Free electrons contribute to the current, causing an increase in electrical conductivity. In addition, it was observed that the Ag/coronene/CdO/Ag hybrid heterojunction under zero potential behaved as a self-powered photodiode. Self-powered photodiodes are optoelectronic materials that can work by themselves without external power and have attracted a lot of attention recently [57, 58]. In the self-powered region of Fig. 9, it converted the light falling on the heterojunction into an electrical signal without the need for external voltage. In addition, this signal became stronger with increasing light intensity.

Photodetectors are devices that convert light energy into electrical energy. The operation of the device basically includes three processes: generation of photogenerated carriers by incident light, transport of photogenerated carriers with any impingement by the current–gain mechanism (if any) and extraction of end electrode to provide the charge carrier output signal [59]. Photodetector parameters of Ag/coronene/CdO/Ag hybrid heterojunction were calculated with: photocurrent I_{ph} ($I_{ph} = I_{ill} - I_{dark}$), responsivity ($R = I_{ph} \cdot P_{inc}^{-1} \cdot A^{-1}$), which is the ratio of produced photocurrent to incoming optical power, sensitivity $S = R \cdot T \cdot V^{-1}$ and specific detectivity characterizing how well a weak signal can be detected compared to detector noise $D^* = R \cdot [A \cdot (2qI_{dark})^{-1}]^{1/2}$

Table 1 Diode parameters of Ag/coronene/CdO/Ag hybrid heterojunction calculated by different methods

Diode	Cheung–Cheung method				Conventional method			$R_j = \frac{\partial V}{\partial I}$	
	$(d(V)/d \ln(I)-I)$		$H(I)-I$		$(\ln(I)-V)$			$R_s(\Omega)$	$R_{sh}(\Omega)$
	n	$R_s(\Omega)$	ϕ_B (eV)	$R_s(\Omega)$	n	$I_0(A)$	ϕ_B (eV)		
Ag/coronene/CdO/Ag	8.57	17×10^3	0.37	1.8×10^3	7.58	3.06×10^{-8}	0.75	2.6×10^3	5.3×10^5

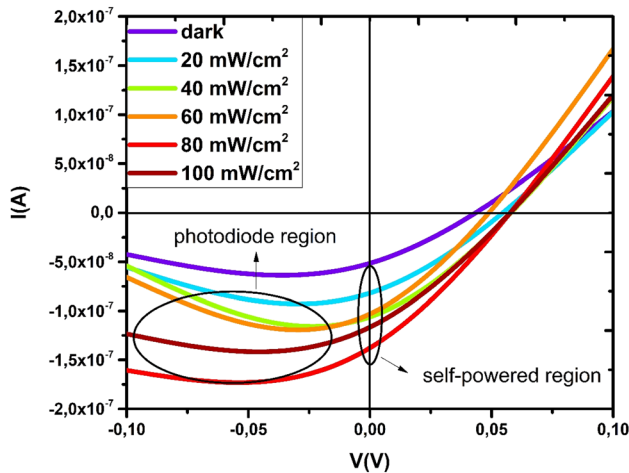


Fig. 9 I–V characteristic of Ag/coronene/CdO/Ag hybrid heterojunction under different light intensities

[30, 31, 60–62]. Here, I_{ill} is the current under the light, I_{dark} is the current in the dark environment, P_{inc} is the light intensity, A is the active contact area, T is the thickness of the active layer and V is the applied voltage.

In Fig. 10a, the graph of I_{ph} against different light intensities is given at -0.1 V, zero bias and 0.1 V applied potentials of the Ag/coronene/CdO/Ag hybrid heterojunction. I_{ph} values were between the range of 1.29×10^{-8} A and 2.03×10^{-7} A at -0.1 V potential, 2.34×10^{-8} and 7.9×10^{-8} A at zero bias and 5.67×10^{-10} A and 6.36×10^{-8} A at 0.1 V potential. The highest I_{ph} values were observed at -0.1 V potential under high light intensity. This indicates that the Ag/coronene/CdO/Ag hybrid heterojunction at high light intensity exhibits typical photodiode behavior operating in reverse bias. The highest I_{ph} values in the low-light-intensity region were seen in zero bias. This means that the self-powered mode of the Ag/coronene/CdO/Ag hybrid heterojunction is more dominant at low light intensity. While maximum I_{ph} values under reverse bias and zero bias were observed under 80 mW.cm^{-2} light intensity, the

maximum I_{ph} value under forward bias was seen at 60 mW.cm^{-2} light intensity. These maximum values are due to the photogenerated carriers reaching their maximum saturation point. In Fig. 10b, the R graph of Ag/coronene/CdO/Ag hybrid heterojunction against different light intensities is given at -0.1 V, zero bias and 0.1 V applied potentials. R values were between $1.03 \times 10^{-2} \text{ A.W}^{-1}$ and $3.72 \times 10^{-2} \text{ A.W}^{-1}$ under -0.1 V potential, $0.73 \times 10^{-2} \text{ A.W}^{-1}$ and $1.52 \times 10^{-2} \text{ A.W}^{-1}$ in zero bias and $0.3 \times 10^{-3} \text{ A.W}^{-1}$ and $1.35 \times 10^{-2} \text{ A.W}^{-1}$ at 0.1 V potential. Calculated R values were found to be higher than phosphorene/metal heterojunction [63], p-Si/Fe(II)-polymeric complex/Au diode [31] values. Under reverse bias, the R-value reached its maximum value under 80 mW.cm^{-2} light intensity and then decreased sharply. The maximum R-value was observed at 60 mW.cm^{-2} light intensity under forward bias and started to decrease after this value. This may be due to the reduction in the light absorption with a radial variation of light intensity [30]. High R values were observed under zero bias in the low-light-intensity region. In Fig. 10c, the S plot of Ag/coronene/CdO/Ag hybrid heterojunction is given against different light intensities at -0.1 and 0.1 V applied potentials. The S values were between $8.56 \times 10^{-9} \text{ S.m.W}^{-1}$ and $7.44 \times 10^{-8} \text{ S.m.W}^{-1}$ under reverse bias and $8.31 \times 10^{-10} \text{ S.m/W}$ and $3.11 \times 10^{-8} \text{ S.m.W}^{-1}$ under forward bias. In Fig. 10d, D^* plot of Ag/coronene/CdO/Ag hybrid heterojunction against different light intensities is given at -0.1 V, zero bias and 0.1 V applied potentials. It has values between 2.83×10^7 Jones and 2.46×10^8 Jones at -0.1 V applied potential, 4.80×10^9 Jones and 9.94×10^9 Jones in zero bias and 1.76×10^6 Jones and 6.57×10^7 Jones at 0.1 V applied potential. It is seen that D^* values in zero bias are quite higher than all light intensity values. This means that the fabricated Ag/coronene/CdO/Ag hybrid heterojunction will be better to detect the incoming signal under zero bias.

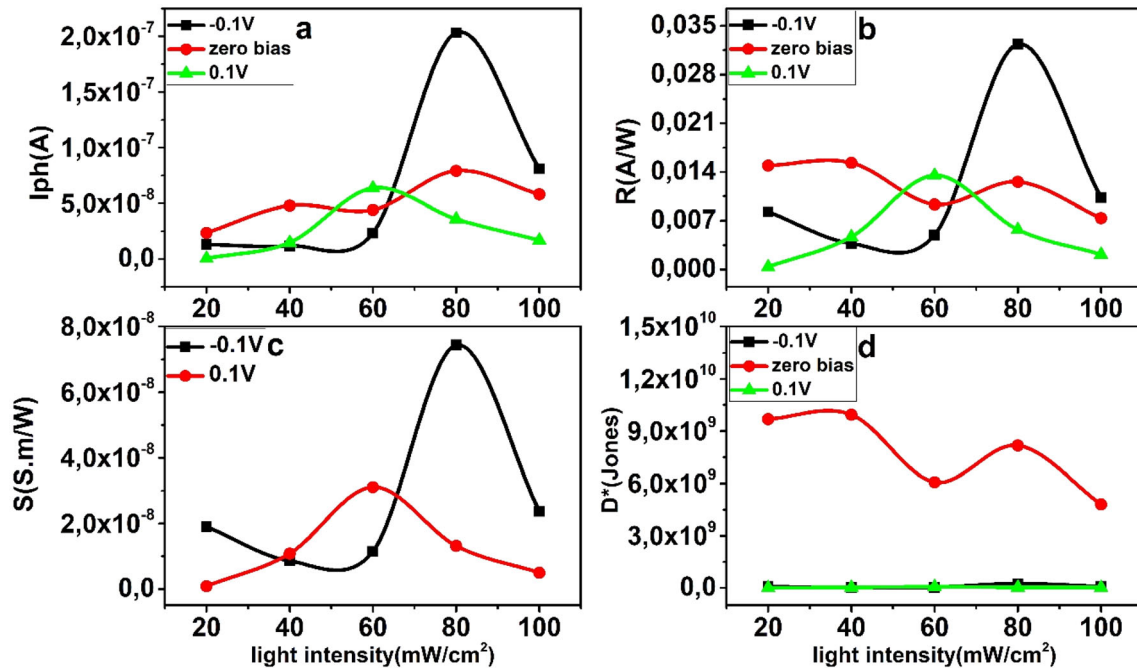


Fig. 10 Photodetector parameters of Ag/coronene/CdO/Ag hybrid heterojunction **a** I_{ph} , **b** R , **c** S and **d** D at reverse bias, zero bias and forward bias under different light intensities

Table 2 shows the graph of the change of photovoltaic parameters of Ag/coronene/CdO/Ag hybrid heterojunction according to light intensity. The fill factor (FF) is calculated from Eq. 8 [64, 65].

$$FF\% = \frac{I_{mp} \times V_{mp}}{I_{sc} \times V_{oc}} \times 100 \quad (8)$$

Here is I_{mp} maximum power point current, V_{mp} is the maximum power point voltage, I_{sc} is the short-circuit current and V_{oc} is open-circuit voltage. It is seen that both I_{sc} and V_{oc} values increase with increasing light intensity. It was observed that the calculated V_{oc} values were higher than the V_{oc} values and lower than the I_{sc} values of the WO_x/Si heterojunction [65]. The Ag/coronene/CdO/Ag hybrid heterojunction we produced showed gain in both current and the maximum open-circuit voltage which occurs when no current flows. The maximum FF%

value was seen at 40 $mW \cdot cm^{-2}$ where the maximum V_{oc} was seen. FF values found were higher than aluminum 8-hydroxyquinoline (Alq3)-based photodiode [66]. FF% values are lower than commercial photovoltaic cells. The inability to determine the appropriate thickness of the layers forming the joints, the wide depletion region between the two layers and the undesirable impurity conditions during production caused the FF value to be low [61].

4 Conclusion

For the first time, metal oxide-based CdO and coronene organic semiconductor interface layer were successfully produced as a heterojunction. According to the electrical analyses in the dark and at different light intensities, it was observed that the hybrid

Table 2 Photovoltaic parameters of Ag/coronene/CdO/Ag hybrid heterojunction

Light intensity ($mW \cdot cm^{-2}$)	I_{sc} (A)	I_{mp} (A)	V_{oc} (V)	V_{mp} (V)	FF%
0	5.80×10^{-8}	–	0.043	–	–
20	8.14×10^{-8}	4.90×10^{-8}	0.054	0.027	3.01×10^1
40	1.06×10^{-7}	6.22×10^{-8}	0.058	0.031	3.14×10^1
60	1.02×10^{-7}	5.73×10^{-8}	0.049	0.026	2.98×10^1
80	1.37×10^{-7}	8.09×10^{-8}	0.057	0.028	2.86×10^1
100	1.16×10^{-7}	6.16×10^{-8}	0.057	0.032	2.94×10^1

heterojunction showed rectifying properties, and the NDR effect was observed between 0.4 and 0.5 V. Besides, it exhibited typical photodiode behavior under reverse bias and self-powered photodiode behavior at zero bias. It was observed that I_{sc} value of fabricated photodiode was raised 2.3 times by the increase in the light intensity at zero bias. Maximum I_{ph} (2.03×10^{-7} A), R (3.72×10^{-2} A.W⁻¹) and S (7.44×10^{-8} S.m.W⁻¹) values were obtained at 80 mW.cm⁻² light intensity. The specific detectivity of the generated heterojunction to incoming signals at all light intensities was observed to be more effective at zero potential. In addition, V_{oc} values of the heterojunction was increased from 0.043 to 0.058 V with the light intensity. Consequently, it is observed that the coronene/CdO hybrid heterojunction exhibited exceptional behavior such as NDR and showed high response to light so it offers an alternative to the field of optoelectronic application.

Nanostructural photodetectors that can convert light into electrical signals have great importance for applications in many fields such as imaging techniques and light wave communication as a new field in nanotechnology-related research. It is clear that the this research in this regard would encourage relevant practical applications.

Author contributions

FU was involved in conceptualization, formal analysis, investigation, methodology, project administration, resources, software, validation, visualization, writing the draft, and writing, reviewing and editing. MŞK was responsible for investigation, methodology, resources, visualization, writing the original draft, and writing, reviewing and editing. SA participated in methodology, resources, visualization, writing the original draft, and writing, reviewing and editing. MK took part in investigation, methodology, resources, writing the original draft, and writing, reviewing and editing.

Funding

The authors have not disclosed any funding.

Data availability

All data generated or analyzed during this study are included in this published article.

Declarations

Conflict of interest This article is original. The article has been written by the stated authors that are all aware of its content and approve its submission. The article has not been published previously. The article is not under consideration for publication elsewhere. No conflict of interest exists, or if such conflict exists, the exact nature must be declared. If accepted, the article will not be published elsewhere in the same form, in any language, without the written consent of the publisher.

References

1. B.G. Lewis, D.C. Paine, Applications and processing of transparent conducting oxides. *MRS Bull.* **25**(8), 22–27 (2000)
2. A. Altuntepe et al., Hybrid transparent conductive electrode structure for solar cell application. *Renewable Energy* **180**, 178–185 (2021)
3. R.J. Wu et al., A selective methane gas sensor based on metal oxide semiconductor equipped with an on-chip microfilter. *Sens. Actuators B Chem.* **359**, 131557 (2022)
4. R. Chandiramouli, B.G. Jeyaprakash, Review of CdO thin films. *Solid State Sci.* **16**, 102–110 (2013)
5. J. Tao et al., Investigation of growth characteristics, compositions, and properties of atomic layer deposited amorphous Zn-doped Ga₂O₃ films. *Appl. Surf. Sci.* **476**, 733–740 (2019)
6. J.-J. Tao et al., Modification of 1D TiO₂ nanowires with GaO x N y by atomic layer deposition for TiO₂@ GaO x N y core-shell nanowires with enhanced photoelectrochemical performance. *Nanoscale* **12**(13), 7159–7173 (2020)
7. İ Orak et al., The diode and photodiode performances of BaZrO₃ perovskite-based device under the influence of thermal and light external stimuli. *Sens. Actuators, A* **337**, 113413 (2022)
8. S.R. Yousefi et al., Dy₂BaCuO₅/Ba₄DyCu₃O₉.09 S-scheme heterojunction nanocomposite with enhanced photocatalytic and antibacterial activities. *J. Am. Ceram. Soc.* **104**(7), 2952–2965 (2021)
9. I.L.P. Raj et al., A comprehensive study on effect of annealing on structural, morphological and optical properties of CdO and photodetection of heterojunction n-CdO/p-Si diode. *Optik* **241**, 166406 (2021)

10. K. Choudhary et al., Sustainable behavior of cauliflower like morphology of Y-doped ZnO: CdO nanocomposite thin films for CO₂ gas sensing application at low operating temperature. *J. Alloys Compounds* **879**, 160479 (2021)
11. P. Sakthivel et al., Radio frequency magnetron sputtered CdO thin films for optoelectronic applications. *J. Phys. Chem. Solids* **126**, 1–10 (2019)
12. H.B. Lu et al., Fabrication of CdO nanotubes via simple thermal evaporation. *Mater. Lett.* **62**(24), 3928–3930 (2008)
13. K. Sirohi et al., Synthesis and characterization of CdO–SnO₂ nanocomposites prepared by hydrothermal method. *Acta Metallurgica Sinica (English Letters)* **31**(3), 254–262 (2017)
14. S.R. Yousefi et al., Hydrothermal synthesis of DyMn₂O₅/Ba₃Mn₂O₈ nanocomposite as a potential hydrogen storage material. *Int. J. Hydrogen Energy* **44**(43), 24005–24016 (2019)
15. T. Singh, D.K. Pandya, R. Singh, Annealing studies on the structural and optical properties of electrodeposited CdO thin films. *Mater. Chem. Phys.* **130**(3), 1366–1371 (2011)
16. F. Roth et al., Electronic structure of undoped and potassium-doped coronene investigated by electron energy-loss spectroscopy. *Phys. Rev. B* (2012). <https://doi.org/10.1103/PhysRevB.85.014513>
17. W.M. Haynes, D.R. Lide, T.J. Bruno, *CRC handbook of chemistry and physics* (CRC Press, 2016)
18. A.D. Chanyshvili et al., Transition from melting to carbonization of naphthalene, anthracene, pyrene and coronene at high pressure. *Phys. Earth Planet. Inter.* **270**, 29–39 (2017)
19. M.M. El-Nahass, H.A.M. Ali, Temperature dependent I–V characterization of Coronene/p-Si based heterojunctions: space charge limited current, Schottky emission at high voltages, thermionic emission and pool-Frenkel emission at low voltages. *Solid State Sci.* **106**, 106297 (2020)
20. M.O. Erdal, Photoresponse properties of coronene nanowires thin-film-based photodiode. *J. Mater. Sci.: Mater. Electron.* **31**(21), 18980–18987 (2020)
21. J. Xiao et al., Preparation, characterization, and photo-switching/light-emitting behaviors of coronene nanowires. *J. Mater. Chem.* **21**(5), 1423–1427 (2011)
22. Ünal, F., ITO cam üzerine büyütülen InSe/rubrene, CIS/rubrene, CIGS/rubrene, InSe/coronene, CIS/coronene, CIGS/coronene heteroeklemlerin yapısal, optik ve elektriksel özelliklerinin belirlenmesi, 2021.
23. S. Saha et al., Electrodeposition of Cadmium from Lewis basic hydrophobic room-temperature ionic liquid. *Electrochemistry* **86**(5), 229–234 (2018)
24. F. Ünal, S. Demir, H. Mammadov, Structural, surface morphological, optical and electrical properties of In_xSe_y thin films, an absorber layer for photovoltaic cells fabricated by M-CBD method using different variables. *Turk. J. Chem.* **45**(6), 1761–1773 (2021)
25. M. Zurnacı et al., Synthesis of a new 1, 3, 4-thiadiazole-substituted phenanthroimidazole derivative, its growth on glass/ITO as a thin film and analysis of some surface and optoelectronic properties. *New J. Chem.* **45**(48), 22678–22690 (2021)
26. S. Aktaş, F. Ünal, Investigation of structural and electrical properties of metal oxide and organic based multi heterojunction. *Karadeniz Fen Bilimleri Dergisi* **12**(1), 508–520 (2022)
27. D. Dwivedi, B. Singh, M. Dubey, Structural and optical investigations of Cd_{1-x}Zn_xTe thin film. *J. Non-Cryst. Solids* **356**(31–32), 1563–1568 (2010)
28. F. Kırmızıgül, E. Güneri, C. Gümüş, Effects of different deposition conditions on the properties of Cu₂S thin films. *Phil. Mag.* **93**(5), 511–523 (2013)
29. A. Yeşildağ et al., Optical and electrical properties of pyrene-imine organic interface layer based on p-Si. *J. Electron. Mater.* **50**(11), 6448–6458 (2021)
30. A. Patel et al., Fabrication, photoresponse and temperature dependence of n-VO₂/n-MoSe₂ heterojunction diode. *Superlattices Microstruct.* **130**, 160–167 (2019)
31. B. Gündüz et al., The photo-electrical properties of the p-Si/Fe(II)-polymeric complex/Au diode. *Synth. Met.* **184**, 73–82 (2013)
32. M.M. El-Nahass, H.A.M. Ali, Temperature dependent I–V characterization of Coronene/p-Si based heterojunctions: space charge limited current, Schottky emission at high voltages, thermionic emission and pool-Frenkel emission at low voltages. *Solid State Sci.* **106**, 106297 (2020)
33. H.G. Çetinkaya et al., Photovoltaic characteristics of Au/PVA (Bi-doped)/n-Si Schottky barrier diodes (SBDs) at various temperatures. *Curr. Appl. Phys.* **13**(6), 1150–1156 (2013)
34. V. Rajagopal Reddy et al., Electrical and carrier transport properties of Ti/α-amylase/p-InP MPS junction with a α-amylase polymer interlayer. *J. Mater. Sci.: Mater. Electron.* **32**, 1–14 (2021)
35. T.U. Kampen, S. Park, D.R.T. Zahn, Barrier height engineering of Ag/GaAs(100) Schottky contacts by a thin organic interlayer. *Appl. Surf. Sci.* **190**(1), 461–466 (2002)
36. Y. Vaknin, R. Dagan, Y. Rosenwaks, Schottky barrier height and image force lowering in monolayer MoS₂ field effect transistors. *Nanomaterials* **10**(12), 2346 (2020)
37. A. Kastalsky et al., Negative-resistance field-effect transistor grown by organometallic chemical vapor deposition. *Solid-State Electron.* **29**(10), 1073–1077 (1986)
38. Ş Aydoğan, *Katıhal Fiziği* (Nobel Akademik Yayıncılık, 2014)

39. P. Bedrossian et al., Demonstration of the tunnel-diode effect on an atomic scale. *Nature* **342**(6247), 258–260 (1989)
40. O. Yilmazoglu et al., First observation of bias oscillations in GaN Gunn diodes on GaN substrate. *IEEE Trans. Electron Devices* **55**(6), 1563–1567 (2008)
41. S. Rehman et al., Current rectification, resistive switching, and stable NDR effect in BaTiO₃/CeO₂ heterostructure devices. *Adv. Electron. Mater.* **7**(6), 2001237 (2021)
42. J.-C. Li, X. Gong, Diode rectification and negative differential resistance of dipyrimidinyl–diphenyl molecular junctions. *Org. Electron.* **14**(10), 2451–2458 (2013)
43. Ş Aydoğan, Ö. Güllü, A. Türüt, Fabrication and electrical characterization of a silicon Schottky device based on organic material. *Phys. Scr.* **79**(3), 035802 (2009)
44. I. Missoum et al., Microelectronic properties of organic Schottky diodes based on MgPc for solar cell applications. *Synth. Met.* **214**, 76–81 (2016)
45. M. Pope, C.E. Swenberg, *Electronic processes in organic crystals and polymers*, vol. 56 (Oxford University Press on Demand, 1999)
46. Ş Aydoğan et al., Extraction of electronic parameters of Schottky diode based on an organic Orcein. *Microelectron. Eng.* **87**(12), 2525–2530 (2010)
47. Ö. Güllü, Ş Aydoğan, A. Türüt, Fabrication and electrical characteristics of Schottky diode based on organic material. *Microelectron. Eng.* **85**(7), 1647–1651 (2008)
48. Z. Liu et al., Temperature-dependent charge transport in Al/Al nanocrystal embedded Al₂O₃ nanocomposite/p-Si diodes. *ECS Solid State Lett.* **1**(1), Q4–Q7 (2012)
49. M.A. Lampert, R.B. Schilling, Chapter 1 current injection in solids: the regional approximation method, in *Semiconductors and semimetals*. ed. by R.K. Willardson, A.C. Beer (Elsevier, 1970), pp.1–96
50. Z. Çaldıran et al., Space charge limited current mechanism (SCLC) in the graphene oxide–Fe₃O₄ nanocomposites/n-Si heterojunctions. *J. Alloy. Compd.* **631**, 261–265 (2015)
51. A. Shetty et al., Temperature dependent electrical characterisation of Pt/HfO₂/n-GaN metal-insulator-semiconductor (MIS) Schottky diodes. *AIP Adv.* **5**(9), 097103 (2015)
52. F. Ünal, M.S. Kurt, S. Durdu, Investigation of the effect of light on the electrical parameters of Si/TiO₂ heterojunctions produced by anodic oxidation on p-type Si wafer. *J. Mater. Sci.: Mater. Electron.* **33**, 15834–15847 (2022)
53. Ünal, F., S. Aktaş, Electrical characterization of n-type doped metal oxide/p-type Si Photosensitive Heterojunction. *J. Inst. Sci. Technol.* 1506–1517 (2022).
54. H.M.J. Al-Ta'ii, V. Periasamy, Y.M. Amin, Electronic characterization of Au/DNA/ITO metal-semiconductor-metal diode and its application as a radiation sensor. *PLOS ONE* **11**(1), e0145423 (2016)
55. S.K. Cheung, N.W. Cheung, Extraction of Schottky diode parameters from forward current-voltage characteristics. *Appl. Phys. Lett.* **49**(2), 85–87 (1986)
56. A. Farag, Structure and transport mechanisms of Si/porous Si n–p junctions prepared by liquid phase epitaxy. *Appl. Surf. Sci.* **255**(6), 3493–3498 (2009)
57. L. Peng, L. Hu, X. Fang, Energy harvesting for nanostructured self-powered photodetectors. *Adv. Func. Mater.* **24**(18), 2591–2610 (2014)
58. W. Tian et al., Self-powered nanoscale photodetectors. *Small* **13**(45), 1701848 (2017)
59. Photodetectors and solar cells. In *Physics of semiconductor devices*, pp. 663–742 (2006).
60. X. Zhang, X. Zhang, L. Wang, Y. Wu, Y. Wang, P. Gao, Y. Han, J. Jie, ZnSe nanowire/Si p-n heterojunctions: device construction and optoelectronic applications. *Nanotechnology* **24**(39), 395201 (2013). <https://doi.org/10.1088/0957-4484/24/39/395201>
61. D. Kaur, M. Kumar, A strategic review on gallium oxide based deep-ultraviolet photodetectors: recent progress and future prospects. *Adv. Optic. Mater.* **9**(9), 2002160 (2021)
62. F. Ünal, Investigation of diode parameters of photoconductive and photovoltaic p-Type Si/Ge-doped WO_x heterojunction. *J. Electron. Mater.* **51**, 6397–6409 (2022)
63. M. Farbod, R. Taheri, A. Kosarian, High performance photoresponsivity and high frequency of phosphorene/metal heterojunction as Schottky photodiode rectifier. *Appl. Mater. Today* **24**, 101092 (2021)
64. D. Bartesaghi et al., Competition between recombination and extraction of free charges determines the fill factor of organic solar cells. *Nat. Commun.* **6**(1), 7083 (2015)
65. S. Aktas, Electrical characterisation of photosensitive Si/W–Ge oxide composite heterojunction. *Opt. Mater.* **132**, 112839 (2022)
66. O. Sevgili et al., Characterization of aluminum 8-hydroxyquinoline microbelts and microdots, and photodiode applications. *J. Phys. Chem. Solids* **136**, 109128 (2020)

Publisher's Note Springer Nature remains neutral with regard to jurisdictional claims in published maps and institutional affiliations.

Springer Nature or its licensor holds exclusive rights to this article under a publishing agreement with the author(s) or other rightsholder(s); author self-archiving of the accepted manuscript version of this article is solely governed by the terms of such publishing agreement and applicable law.